

Article

Marine Stratus—A Boundary-Layer Model

Peter A. Taylor 

Earth and Space Science and Engineering, York University, Toronto, ON M3J 1P3, Canada; pat@yorku.ca

Abstract: A relatively simple 1D RANS model of the time evolution of the planetary boundary layer is extended to include water vapor and cloud droplets plus transfers between them. Radiative fluxes and flux divergence are also included. An underlying ocean surface is treated as a source of water vapor and as a sink for cloud or fog droplets. With a constant sea surface temperature and a steady wind, initially dry or relatively dry air will moisten, starting at the surface. Turbulent boundary layer mixing will then lead towards a layer with a well-mixed potential temperature (and so temperature decreasing with height) and well-mixed water vapor mixing ratio. As a result, the air will, sooner or later, become saturated at some level, and a stratus cloud will form.

Keywords: model; boundary layer; marine stratus cloud

1. Introduction

It is clear from Figure 1 that cloud cover is high over mid-latitude ocean surfaces. In collaboration with the Fatima [1] project, my group at York University has been studying and forecasting fog occurrence over the Canadian, coastal N. Atlantic, and over the Yellow Sea near Korea. Our early studies [2,3] with the forecast model, WRF, introduced the idea that the ocean water surface should be a sink for cloud droplets as well as a source for water vapor. In parallel with our WRF modeling, we have developed a separate boundary-layer cloud model.



Citation: Taylor, P.A. Marine Stratus—A Boundary-Layer Model. *Atmosphere* **2024**, *15*, 585. <https://doi.org/10.3390/atmos15050585>

Academic Editors: Jianhao Zhang, Hendrik Andersen, Tom Goren and Yubin Li

Received: 20 February 2024

Revised: 6 May 2024

Accepted: 8 May 2024

Published: 11 May 2024



Copyright: © 2024 by the author. Licensee MDPI, Basel, Switzerland. This article is an open access article distributed under the terms and conditions of the Creative Commons Attribution (CC BY) license (<https://creativecommons.org/licenses/by/4.0/>).

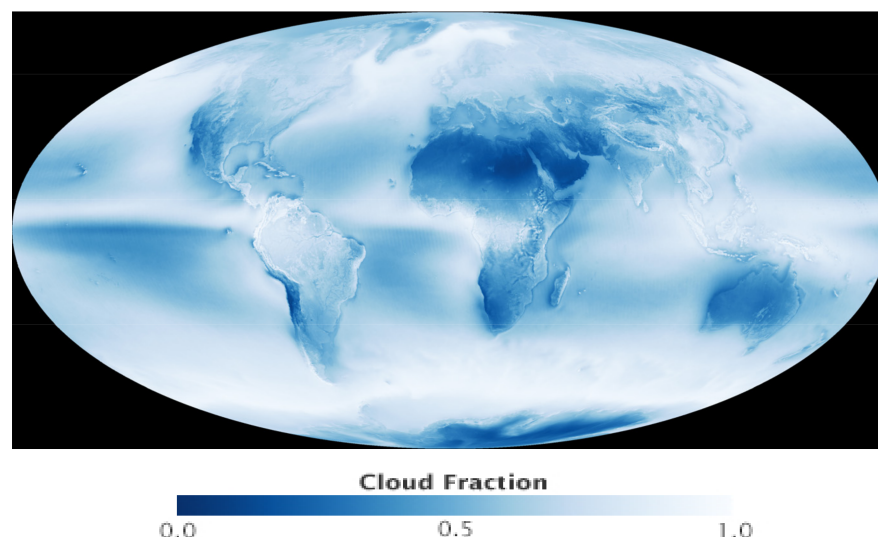


Figure 1. Global cloud coverage, from <https://earthobservatory.nasa.gov/images/85843/cloudy-earth> (accessed on 1 May 2024).

It is important to stress that the model used here is a relatively simple “toy” model that we are using to explore processes involved in boundary-layer clouds and fog. While others are using 3D high resolution, large eddy simulation models, there is a lot that can be learned

from simpler Reynolds-Averaged Navier–Stokes equation (RANS) models and idealized one dimensional situations with assumed horizontal homogeneity. In my group, we also use the Weather Research and Forecasting (WRF) model in both Single Column and 3D forecast modes. Within WRF, just the microphysics module (mp_thompson) has 5470 lines of code and tracking down exactly how things work is not easy! Warm clouds are easier than cold ones, and we also simplify vapor–droplet transitions. These are assumed to occur instantaneously, and we do not have droplet–drizzle–rain transitions—it is a simple model.

In a steady, well-mixed turbulent boundary layer above a water surface, potential temperature (Θ) and water vapor mixing ratio (Q) should, over time, become equal to surface values. The atmospheric boundary layer over the ocean is often capped by stable stratification above 1–2 km, and winds can be strong (of order 20 ms^{-1}). Sample profiles from Sable Island (WSA) are shown in Figure 2. In this case, we see that clouds would have been present from about 500–1250 m with a stable layer at the top. Note that, sadly, the Sable Island radiosonde program ended in 2019 [4].

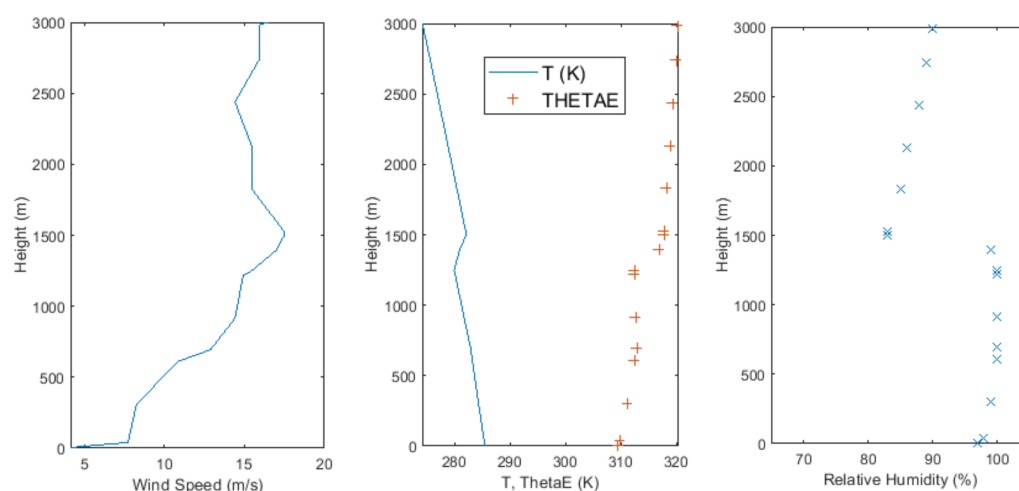


Figure 2. Wind speed, temperature and humidity profiles on a cloudy day over Sable Island, 00Z, 3 July 2019, data from <http://weather.uwyo.edu/upperair/sounding.html> (accessed on 19 February 2024). Note Θ_e , ThetaE, is the equivalent potential temperature with the latent heat of water vapor accounted for.

With potential temperature, $\Theta(z) \approx \Theta(0)$, and unsaturated air with the dry adiabatic lapse rate, $\Gamma (= 9.8 \text{ K/km})$, we might expect $T(z) \approx T(0) - \Gamma z$, and as a result, the saturation vapor pressure and saturation mixing ratio will decrease with z . In the plots above, the lapse rate is lower ($\sim 4 \text{ K/km}$), but the upward mixing of water vapor would still lead to condensation at some level. Since we are assuming saturation at the water surface, we might expect this to start as a surface-based cloud, but the water vapor is mixing upwards, and clouds will initially form higher up. There may be close to 100% relative humidity (RH) in the lower layers of the boundary layer, but the liquid water mixing ratio (QL) is assumed to be 0 at $z = 0$, and any liquid water would be diffused towards the surface. Katata [5,6] used similar ideas about droplet deposition over vegetation and forests.

Garratt’s (1992) text on the atmospheric boundary layer [7] includes a chapter on the cloud-topped boundary layer or CTBL. It notes that, “The presence of clouds leads to considerable complications compared to a dry ABL (Atmospheric Boundary Layer) because of the important role played by radiative fluxes and phase changes.” There is an excellent discussion of properties and good examples of observations, but Garratt also includes the statement that “relatively few modelling studies have been made on the CTBL”. However, clouds within the boundary layer include fog, and the paper by Fisher and Caplan in 1963 [8] covers both fog and stratus clouds. They develop a preliminary 1D turbulent diffusion model with water vapor and cloud liquid water included. They note the potential significance of radiational cooling but it was not included in their model. In

their conclusions, they stress the need for field measurements on the vertical profiles of cloud liquid water content. Some have been made [9], but more are still needed 60 years after their work.

Chapter 7 of Cotton and Anthes's 1989 book *Storm and Cloud Dynamics* [10] discusses marine fog and, in particular, the OLV model [11] from 1978. The OLV paper includes predictions of stratus clouds and fogs caused by stratus lowering as well as advective-radiative fogs. It is a RANS model and uses second-order closure, in comparison to our simple model with 1.5-order closure. Radiative flux divergence is included, and vapor-liquid droplet transfers are present within a model with total water and a "conserved" potential temperature (θ_s) as the moisture-related variables. Lower boundary conditions appear to be based on mean surface values of total water mixing ratio and virtual potential temperature (OLW p 305), but it is not clear how liquid water droplets interact with the water surface. Our model will assume that they collide and coalesce so that the water surface is a sink for liquid water in the air ($QL(0) = 0$). Figure 3 of the OLV paper shows maximum values of QL at the surface in a warm surface fog situation (cold air advected over warm water). Our model would remove those surface droplets by coalescence with the underlying water surface.

There have been other model studies of fog and stratus clouds over water and land surfaces since then, including with NWP models, some single-column versions [12], large eddy simulations [13], and comparisons of both with observations. Work by Koraćin et al. [14], based on the Lagrangian advection of a 1D model, has similar features to our model described below, although details (see [15,16]) are different. Koraćin et al. include a large-scale subsidence term, which they see as an important factor in fog caused by stratus lowering. In the coastal California context, they state, "Although the positive fluxes of sensible and latent heat at the air-sea interface are the factors that govern the onset of fog, sensitivity studies with the one-dimensional model indicate that these sensible and latent heat fluxes are of secondary importance as compared to subsidence and cloud-top cooling". In parallel work on advection fog over cooling surfaces, we can form fog without subsidence.

These earlier papers have generally focused on simulating particular cases, and I am not aware of any high-resolution but simple PBL models presenting the basic situations over ocean water surfaces that we will study here.

2. A 1D PBL Model

Starting from the 1D PBL model (WT) developed with Wensong Weng [17], we can add water vapor and liquid water and allow for transfers between them. We have also added radiative fluxes. In an idealized, horizontally homogeneous ABL and in the absence of radiative flux divergence and moisture, the WT Reynolds-averaged equations (RANS) describing the dynamics of the ABL can be written as shown below. In these equations, upper case symbols, \mathbf{U} , V , θ , etc., represent ensemble or Reynolds-averaged quantities. We assume that $W = 0$. Lower case, u , v , w , θ , etc., are turbulent fluctuations, and $\langle \dots \rangle$ represents an ensemble average. Technically, this is over many realizations of the flow, but in this horizontally homogeneous flow situation, it can be a horizontal average at fixed z and t .

$$\frac{\partial \mathbf{U}}{\partial t} = f(V - V_g) - \frac{\partial \langle uw \rangle}{\partial z}, \quad \frac{\partial V}{\partial t} = f(\mathbf{U}_g - \mathbf{U}) - \frac{\partial \langle vw \rangle}{\partial z}, \quad (1)$$

$$\frac{\partial \Theta}{\partial t} = -\frac{\partial \langle w\theta \rangle}{\partial z} + (RFDIV + LHT)/(\rho c_p) \quad (2)$$

$$\frac{\partial E}{\partial t} = P_s + P_b - \epsilon - \frac{\partial \langle we \rangle}{\partial z} \quad (3)$$

Here, $RFDIV$ is radiative flux divergence and LHT is a rate of latent heat release, or demand if negative. These are per unit mass of air. The specific heat of dry air at constant

pressure, c_{pa} , starts as $1005 \text{ J kg}^{-1} \text{ K}^{-1}$ but includes adjustments for temperature, and c_p is for moist air accounting for mixing ratios and specific heats of water vapor and liquid water.

$$c_p = (c_{pa}(T) + Qc_{pv} + QLc_l)/M, \quad \text{in } \text{J kg}^{-1} \text{ K}^{-1} \quad (4)$$

where the total mass of a volume containing 1 kg of dry air, as a mixing ratio, is

$$M = 1.0 + Q + QL = \text{constant}; \quad \text{with } Q \text{ and } QL \geq 0 \quad (5)$$

To these equations, we add conservation equations for water vapor, Q and liquid water, QL mixing ratios, defined in the atmospheric way as mass per unit mass of dry air. These are

$$\frac{\partial Q}{\partial t} = -\frac{\partial \langle wq \rangle}{\partial z} - \Delta Q, \quad (6)$$

$$\text{and} \quad \frac{\partial QL}{\partial t} = -\frac{\partial \langle wql \rangle}{\partial z} - \frac{\partial (W_s QL)}{\partial z} + \Delta Q. \quad (7)$$

Here ΔQ is the rate at which water vapor is condensing into, or evaporating from, cloud droplets. It is dependent on the saturation mixing ratio $QSAT(T)$ and computed at each time step in a subroutine which is called "Adjust". The latent heat added or subtracted in Equation (2), LHT is simply $L\Delta Q$, where L is the latent heat of vaporization (2466 J/g at 288 K , but temperature variations are included). W_s is the gravitational settling velocity of the droplets that are formed. Turbulent fluxes are represented by

$$\begin{aligned} -\langle uw \rangle &= K_m \frac{\partial U}{\partial z}, \quad -\langle vw \rangle = K_m \frac{\partial V}{\partial z}, \quad -\langle w\theta \rangle = K_h \frac{\partial \Theta}{\partial z} \\ -\langle wq \rangle &= K_q \frac{\partial Q}{\partial z}, \quad -\langle wql \rangle = K_{ql} \frac{\partial QL}{\partial z}. \end{aligned} \quad (8)$$

where the eddy diffusivities, K_m , K_h , etc., could differ. In addition, we use an equation for turbulent kinetic energy per unit mass (TKE, $E = 0.5 [\langle u^2 \rangle + \langle v^2 \rangle + \langle w^2 \rangle]$),

$$\frac{\partial E}{\partial t} = P_s + P_b + \frac{\partial}{\partial z} \left(K_m \frac{\partial E}{\partial z} \right) - \varepsilon. \quad (9)$$

Here P_s and P_b are shear and buoyancy production terms, and ε is the rate of viscous dissipation, details in WT. The eddy diffusivities in this basic $E-l$, 1.5 order closure are

$$K_m = l_m (\alpha E)^{1/2}, \quad K_h = \frac{K_m}{Pr}, \quad \text{and} \quad \frac{1}{l_m} = \frac{\phi_m}{\kappa(z+z_0)} + \frac{1}{l_0} \quad (10)$$

Again, more details are in WT, but calculations here use $\alpha = 0.25$, and a Prandtl number, $Pr = 1.0$. We use the same z_0 for all quantities and ϕ_m is a function of z/L_o where L_o is the Obukhov length, based on local shear stress and heat flux values. In neutral stratification, L_o is infinite and $\phi_m = 1$.

Lower boundary conditions on the water surface are $\mathbf{U} = 0$, $\Theta = T_{surf}$, the surface water temperature, $Q = QSAT(T_{surf})$ and $QL = 0$. The surface can thus be a source of water vapor but is assumed to be a sink for cloud droplets as they collide and coalesce. Fluxes of momentum, heat, water vapor and liquid water evolve as a part of the solution and depend on the assumed roughness lengths. These can differ, z_{0m} , z_{0h} , etc., but are presently all set as $z_0 = 0.001 \text{ m}$.

Water droplets can be significant absorbers and emitters of long-wave radiation. For solar radiation, it is sometimes argued that cloud and fog droplets scatter rather than absorb solar radiation and the direct impact may be small. A layer of stratus cloud will, however, significantly reduce downwelling irradiance at the surface, and not all of the downwelling energy is backscattered. One website, <https://www.foxweather.com/learn/does-fog-really-burn-off-dispelling-the-myth-of-combustible-clouds> (accessed on 13 February 2024) states "People commonly refer to the dissipation of fog as 'burning off' but the reality

is much less exciting". Fog will forward scatter much of the solar radiation and, over land, will raise the surface and near-surface air temperatures, causing fog to dissipate. Solar radiation will heat up the upper layers of the ocean, but the increase in sea surface temperature is far less than for land surface temperatures, and, over water, the absorption of solar radiation by cloud and fog droplets may be more relevant. There appears to be limited information on the absorption of solar radiation by cloud droplets [18].

To determine the radiative flux divergence, we need to model the four components of irradiance: RFU and RFD for long waves and SFD and SFU for solar radiation. All may be subject to absorption and there will be emission of long-wave radiation by cloud droplets. There will also be absorption and long-wave emissions by the air but for now, although included in the equations, these will be considered as small background effects compared with the local impact of cloud droplets. We also ignore backscattering and use a simple 2-stream (upwelling and downwelling) approach. With air density ρ_a , and using mass absorption coefficients (k_a, k_w, k_{sa}, k_{sw}), ignoring backscattering, and with σ as the Stefan–Boltzmann constant, we can write the transfer equations for irradiance as,

$$\frac{\partial RFU}{\partial z} = (-RFU + \epsilon\sigma T^4)(QLk_w + k_a)\rho_a, \quad \frac{\partial RFD}{\partial z} = (RFD - \epsilon\sigma T^4)(QLk_w + k_a)\rho_a \quad (11)$$

$$\frac{\partial SFU}{\partial z} = -SFU(QLk_{sw} + k_{sa})\rho_a, \quad \frac{\partial SFD}{\partial z} = SFD(QLk_{sw} + k_{sa})\rho_a \quad (12)$$

Here ρ_a is dry air density. Initially, we neglect clear air absorption ($k_a, k_{sa} = 0$), set the emissivity, $\epsilon = 1$, and focus on absorption coefficients for cloud droplets (k_w, k_{sw}) with units of m^2kg^{-1} . A serious omission is the back scattering and multiple scattering of downwelling solar radiation (SFD) and the contribution to SFU . A more careful treatment of solar radiation is planned for future work.

Boundary conditions are needed on upwelling radiant fluxes at the surface and downwelling fluxes at the model top. These are specified in Section 3.3, based on black body RFU at the water surface and a relatively low albedo (0.05 in cases here) for solar irradiance. At the top boundary (300 m in this case), we specify a typical, clear sky value for RFD (200 Wm^{-2} here) and must specify SFD . In realistic simulations, this will have a strong diurnal cycle, but in the test case considered in Section 3.3, we simply set $SFD = 250 \text{ Wm}^{-2}$ and hold it constant.

The heating term added to Equation (2) is

$$RFDIV = \frac{\partial}{\partial z}(RFD + SFD - RFU - SFU). \quad (13)$$

Our microphysics assumes that condensation occurs instantaneously if the mixing ratio, $Q > QSAT(T)$, the saturation value at air temperature, T . Then Q instantly reduces towards that saturation value with the excess becoming liquid water, QL . This releases latent heat, raises T , and modifies $QSAT$ so that some iteration is needed. An adjustment is made in the opposite direction when liquid droplets diffuse into a sub-saturated layer. A similar approach was used by Brown and Roach [19], but no details were provided. Both transformations are assumed to take place at constant total pressure and with no external source or sink of heat. Our saturation adjustment involves some iteration and is illustrated in Figure 3. QL is not shown but could be computed via Equation (14) below.

The adjustment is between a non-equilibrium state (Q_1, QL_1, T_1) predicted after a time step (Equations (1)–(7)) with $Q_1 \neq QS_1$ to an equilibrium state with $Q_2 = QS_2$, where $QS_i = QS(T_i, P)$, the saturation mixing ratio. Note that no adjustment is needed (Case 1) if $Q_1 < QS_1$ and $QL_1 = 0$, but one is needed (Case 2) if $Q_1 > QS_1$. In Case 4, we may find $Q_1 < QS_1$ and $QL_1 > 0$, and liquid water will evaporate, cooling the air. It may also be possible (Case 3), with $Q_1 < QS_1$ and $QL_1 > 0$, to evaporate all the droplets while $Q_2 < QS_2$. Our approach would then predict $QL_2 < 0$, and adjustments are made to correct for that.

The essential feature of the adjustment is that heat per unit mass of the mass of the material undergoing the adjustment is conserved, i.e.,

$$H = L_1 Q_1 + M c_{p1} T_1 = L_2 Q_2 + M c_{p2} T_2. \tag{14}$$

where c_{p1} and c_{p2} are the specific heats of the dry air plus water vapor and liquid water in states 1 and 2. M is the total mass (dry air plus water vapor and liquid water) per unit mass of dry air, as in Equation (4). This is a constant during the adjustment. In the cases shown, our desired saturation adjustments correspond to the points of intersection of the solid green and blue lines with the black line corresponding to $QS(T)$. If we use the tangent QS line and set $c_p = c_{p1}$ in the $H = \text{constant}$ line, as in our initial estimates of state 2, we get the points of intersection of the dashed lines. Additional details are at <https://www.yorku.ca/pat/AdjustJan2024.pdf> (accessed on 7 May 2024).

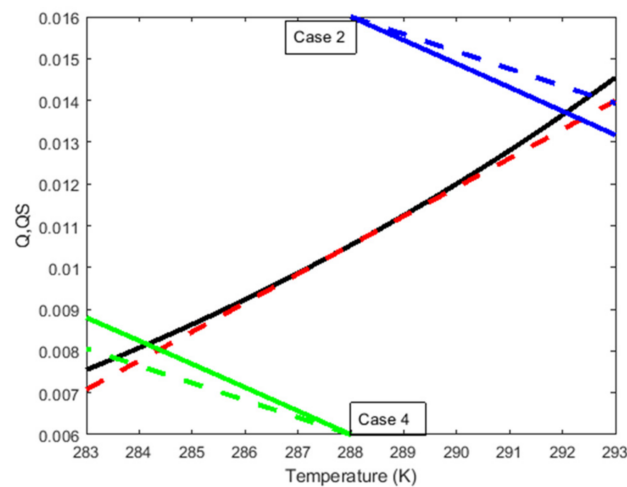


Figure 3. Two saturation adjustment cases (2 and 4) with initial temperature $T_1 = 288$ K plus an illustration of $q_s(T)$ and (dashed red line) the linear approximation $q_{sa}(T)$. The solid blue and green lines correspond to $H = \text{constant}$ in the two cases. The corresponding dashed lines are first approximations with state 1 values of c_p and L and QS varying linearly with T .

3. Results

3.1. Initial States

We can run the model with completely dry air, no clouds, and no radiative fluxes to obtain initial profiles. Initial temperature profiles can be for neutral stratification, or we can specify a weak stable stratification. We used either $d\Theta/dz = 0$ or 2 K/km and used $T_{surf} = 288$ K. We assumed a geostrophic wind $\mathbf{U}_g = (20, 0)$ ms^{-1} with $z_0 = 0.001$ m and Coriolis parameter, $f = 10^{-4} \text{s}^{-1}$. Initial TKE was set to a surface value based on the geostrophic drag law and we imposed an exponential decay with height $\exp(-z/2000)$ m). As initial conditions for these runs, we simply set $\mathbf{U} = \mathbf{U}_g$ at all levels. Initial values are not important—we are just seeking an equilibrium steady state. With neutral stratification, we get a typical Ekman spiral profile while Θ is constant and T decreases at the dry adiabatic lapse rate. Results are in Figure 4 and use 241 vertical levels between the surface and a model top at 3 km. The time step used is 2.5 s, and we impose a TKE (E) minimum of $0.00001 \text{ m}^2 \text{ s}^{-2}$.

With an initial stable lapse rate, the PBL model will evolve to the state shown in Figure 5. Turbulent mixing will lead to a relatively constant well-mixed potential temperature layer up to about 800 m, in this case, capped by a relatively strong stable layer, while above that, the stratification stays at $d\Theta/dz = 2$ K/km. In that layer near $z = 900$ m, there can be strong velocity shear and weak inertial oscillations can persist. We will refer to the final profiles as our “2 K/km stable equilibrium”.

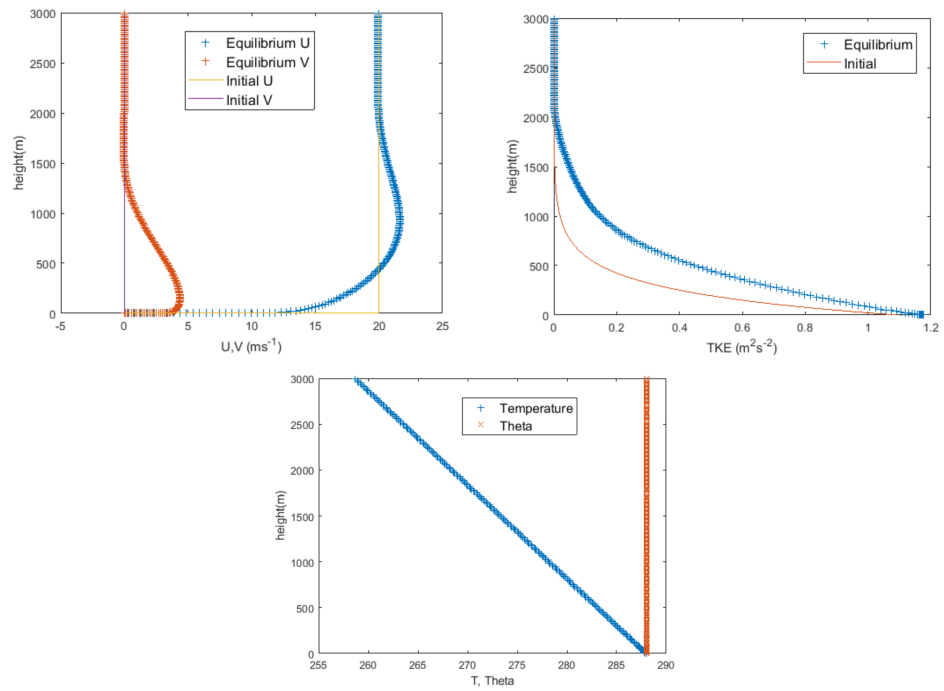


Figure 4. Equilibrium planetary boundary layer profiles with neutral stratification and dry air. Initial state had $\mathbf{U}_g = (20, 0) \text{ ms}^{-1}$ and $\Theta = 288\text{K}$ for all z . Also note $z_0 = 0.001\text{m}$ and $f = 10^{-4}\text{s}^{-1}$. Equilibrium profiles are after integration for 5 days.

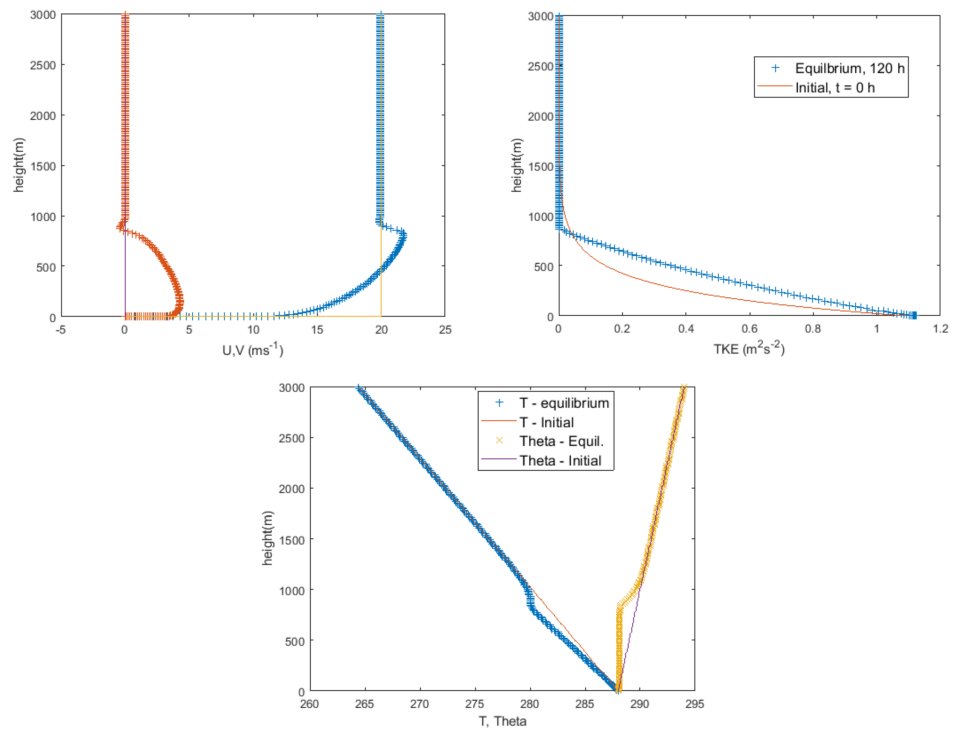


Figure 5. Equilibrium planetary boundary layer profiles with dry air and stable stratification aloft. Our initial state had $\mathbf{U}_g = (20, 0) \text{ ms}^{-1}$ and $\Theta = 288 + 0.002 z \text{ K}$ for all $z(\text{m})$. We use the same initial TKE, $z_0 = 0.001 \text{ m}$ and $f = 10^{-4}\text{s}^{-1}$, as in Figure 4. Surface temperature (T_s) is maintained at 288 K.

3.2. Adding Moisture

We can now restart and continue computations, starting with the \mathbf{U}, V, E, Θ stable layer “2K/km equilibrium” profiles discussed in the previous section as initial conditions and now adding moisture effects, and potential condensation. Results after 5 days are shown in

Figure 6. Our surface boundary conditions will now include mixing ratios $Q = QSAT(T_s)$, $QL = 0$ while T_{surf} is maintained, in this case, at 288 K. We can set initial profiles of Q and QL as we wish, but the extreme case is to have completely dry air with $Q = 0$ for all $z > 0$, and $QL = 0$ for $z \geq 0$. Our air column may have been advected from an extremely dry desert out over an ocean.

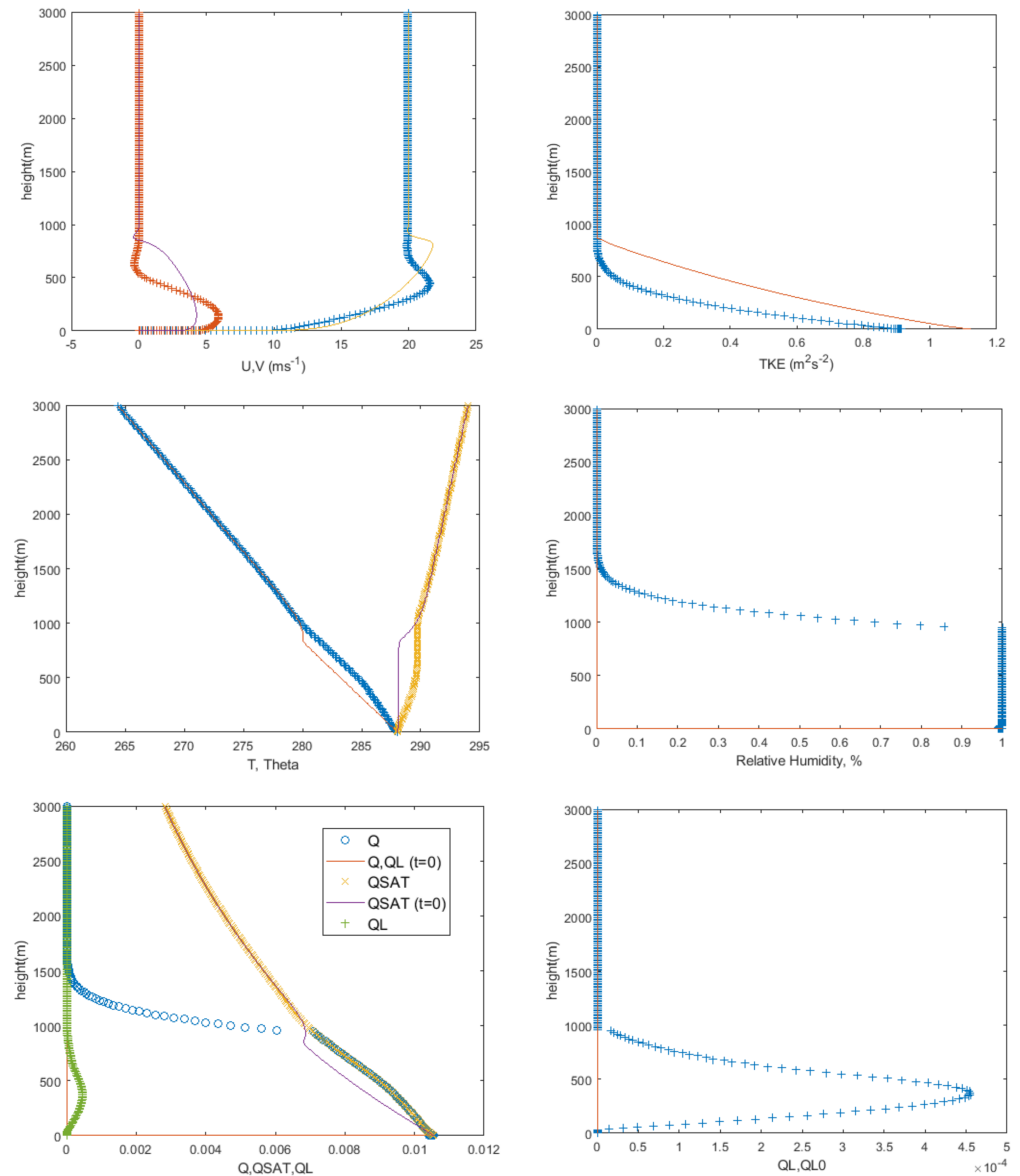


Figure 6. Results after 5 days over a water surface. Thin lines define the initial conditions (equilibrium profiles from Figure 5) and o, +, x symbols are values after 120 h over a water surface with $Q(z = 0) = QSAT(288K)$. Note that temperature and potential temperature are in K, Relative Humidity = 1 is 100% and that mixing ratios, Q , QL , $QSAT$ are in kg/kg.

During the 5 days, starting with $RH = 0$, water vapor diffuses upwards from the water surface, some condenses and warms the air. In these results, after 5 days, a cloud extends from near the surface ($z \sim 30$ m) to about $z = 944$ m, as shown by the RH and QL profiles. Note that there is significant variation in QL within the $RH = 1.0$ layer, and the QL maximum (about 0.45 g/kg) is far less than that of the Q and $QSAT$ values, which are of order 10 g/kg at the same level. We can allow some gravitational settling of the cloud/fog droplets. In the plots shown, we applied a settling velocity, W_s , of 0.005 ms^{-1} , appropriate to droplets of diameter near 13 μm . Gravitational settling over a day would

lead to a descent of 432 m, so it can play a significant role and there will be some sensitivity to the value used.

The droplet formation seems to have occurred through the upper part of the boundary layer, leading to heating by about 1.7 K over the 5 days. This leads to stable stratification in the lower part of the boundary layer and a well-mixed layer above with a top that has risen from about 800 m to 1000 m. Changes in the stratification lead to adjustments of the velocity profiles and weakening of the velocity shear at the boundary-layer top. The *TKE* profile is also smoothed in these upper layers, and *TKE* values are reduced because of stable stratification in the lower part of the boundary layer. *QSAT* profiles are also modified by the temperature change.

In Figure 7, we show the evolution of the *QL* profiles over time, and we have extended the computations to 10 days. In this rather extreme case, starting with completely dry air, no cloud has formed after day 1 but appears during day 2, and clouds are present after 30 h in a layer from 500–890m above the surface. The cloud base lowers with time, and the cloud top rises to about 945 m. The drop in *QL* with height at the cloud top is sharp and stays at about that level for 5 days. Gravitational settling, W_s , does, however, reduce *QL* at the cloud top, and by day 6, there is a smoother transition to clear air above the cloud (Figure 7). If we start with some moisture present, the cloud forms more quickly and initial cloud water mixing ratios are higher.

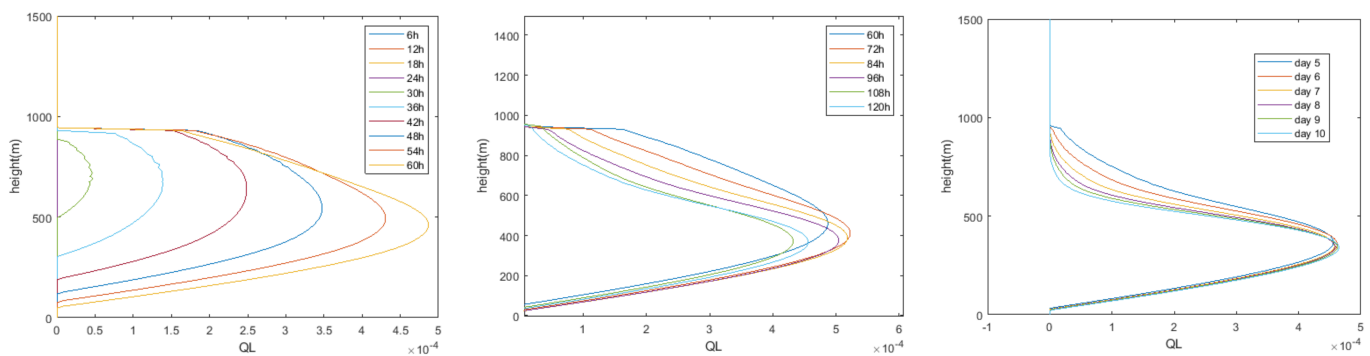


Figure 7. From the same case as in Figure 6, *QL* profiles every 6 h, every 12 h and every 24 h. The first cloud appears after 30 h and a relatively steady profile after 120 h, with a maximum lower than the earlier peak.

If we set $W_s = 0$, we obtain the results shown in Figure 8, extended to 10 days. The first two days are quite similar to the results with $W_s = -0.005 \text{ ms}^{-1}$ shown earlier, but as time moves on, the cloud top continues to rise, and peak *QL* values slowly increase. There is some sensitivity to the treatment of mixing in stable conditions at the top of the cloud.

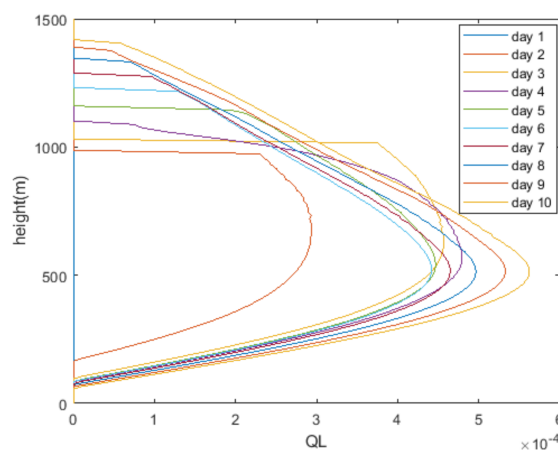


Figure 8. Daily *QL* (kg/kg) profile results with $W_s = 0$.

3.3. Adding Radiation

Radiative flux absorption, in clear air and in clouds, is a complex process with strong and detailed wavelength and droplet size dependence. We use a simple 2-stream approach for irradiance, upwelling and downwelling, long wave (*RFU*, *RFD*), and solar (*SFU*, *SFD*). Basically, we use the radiative transfer equation, or Schwarzschild's equation, integrated over the wavelengths concerned and over the zenith angle, azimuthally averaged, and applied to irradiance. We assume all scattering is forward and that long-wave emissions from cloud droplets produce both upwelling and downwelling long-wave radiation.

One problem with adding radiation effects is finding appropriate grey body irradiance values of the long and short-wave mass absorption cross section coefficients for water droplets, k_w , k_{sw} . Units will be m^2kg^{-1} . Stephens's paper [18], (his Table 3), leads us to use $k_w = 80 \text{ m}^2\text{kg}^{-1}$ for infrared irradiance. For solar radiation, we initially take $k_{sw} = 40 \text{ m}^2\text{kg}^{-1}$, but much deeper investigation is needed. Adjustment for solar angle with the time of day would be needed for *SFD* above, within the cloud, and for k_{sw} , but for now, we will just set these as constant to illustrate potential solar heating effects. As discussed in Section 2 above, we also need to take into account backscattering within the cloud layer, find appropriate coefficients for that, and find a way to treat diurnal cycles.

To illustrate the effects of long-wave radiation, we look at a simple sample case with no solar radiation. Other parameters are as in our "2K/km equilibrium" case, which provides our initial conditions. Downwelling long-wave radiation from the air above the model upper boundary (3 km) is set as 200 Wm^{-2} , and the surface irradiance, at $z = 0 \text{ m}$, is the black body value, in this case at 288 K, 390 Wm^{-2} . Selected results are in Figure 9, extending out to 60 h. Soon after that 60 h point, the model ran into computational problems, probably associated with the extremely strong thermal stability conditions that developed at the cloud top where radiational cooling had dropped the temperature down by about 7 K, as shown in Figure 9a. Results at the 60 h point show upwelling and downwelling long-wave radiation both equal to black body emissions at the cloud water temperature through most of the cloud layer (Figure 9c). Near the cloud base ($\sim 500 \text{ m}$), where *QL* is lower, there is still some unabsorbed radiation from the underlying water surface so that $RFU > RFD$. Clouds appear at around 30 h, as in the case with no radiation, after which the liquid water content of the cloud increases with time (Figure 9b) and has a maximum near the cloud top where radiational cooling is lowering temperatures, as illustrated in Figure 9a. In Figure 9c, one can see that just at the cloud top level, $d(RFD - RFU)/dz$ will be negative, and, with no solar component, *RFDIV* is also negative and will cause the cloud top cooling.

In Figure 9a,d, there are strong variations of *T* and *Q* near the surface due to the upward diffusion of heat and water vapor from the surface source towards the cloud layer, where strong radiational cooling and subsequent condensation occur. Plotting temperature and *Q* profiles against $\ln z$ reveals normal log-linear profiles in the sub-cloud layer (Figure 10) while the cloud top data gets rather compressed.

As an idealized exercise, we add solar radiation effects, ignoring diurnal variations and holding incoming solar radiation constant with time. We assume downwelling solar irradiance at the model top of 250 Wm^{-2} and hold the absorption coefficient, $k_{sw} = 40 \text{ m}^2\text{kg}^{-1}$, constant. In this case, a stable situation develops, and Figure 11 shows results after 5 days of development. The boundary layer cloud develops with a base of around 200 m and extends up to $\sim 1100 \text{ m}$. The *RH* is 1.0 with $Q = \text{QSAT}$ (Figure 11b) throughout the cloud layer, but the liquid water content is low and hardly visible in Figure 11b. With a time step of 2.5 s, results in the upper part of the cloud were a little noisy, so we reduced the time step to 0.25 s for Figure 11c (note also a different *z* scale) above. The maximum *QL* of around 0.03 g/kg can be compared to 0.5 g/kg in the case with no radiation and $\sim 1 \text{ g/kg}$ in the long-wave radiation case. At $t = 5 \text{ days}$, the four irradiance components are shown in Figure 11d.

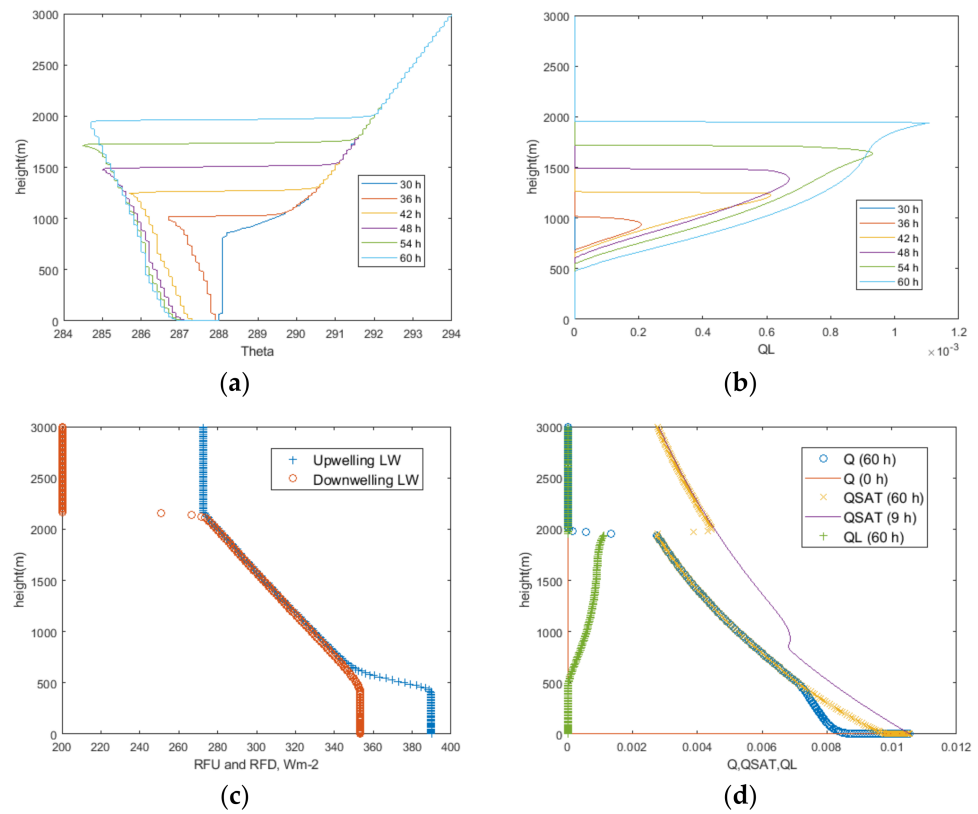


Figure 9. Selected results with long-wave radiation, up to 60 h. (a) Potential temperature (K), (b) Liquid water mixing ratio, QL (kg/kg so 10^{-3} g/kg), (c) Radiative fluxes, long wave, infrared, Wm^{-2} , (d) Mixing ratios, Q , $QSAT$, QL (kg/kg).

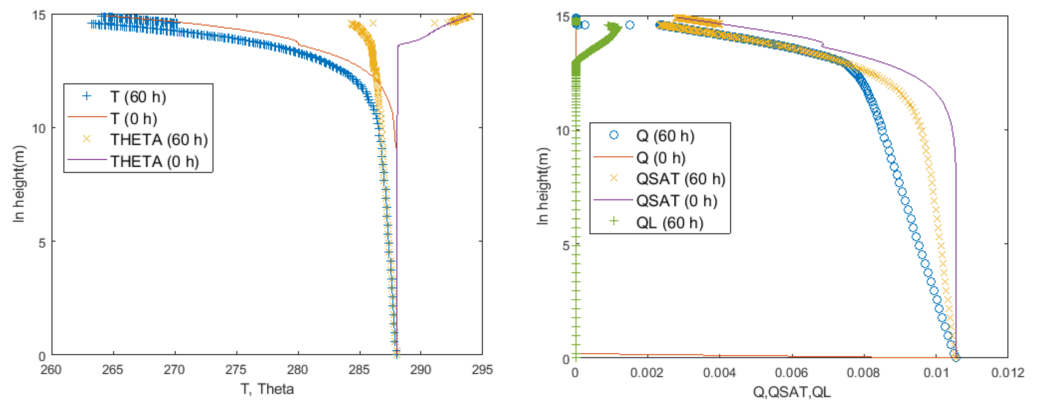


Figure 10. T , Θ (K) and Q , $QSAT$, QL (kg/kg) results with long-wave radiation after 60 h.

In this case, the cloud approaches a relatively steady state in terms of depth after 2 days while QL increases slowly (Figure 11c). If we reduce the solar absorption coefficient, k_{sw} , to $20 \text{ m}^2\text{kg}^{-1}$, the QL values are still low (max $\sim 0.1 \text{ g/kg}$), and the depth increases steadily with time ($\sim 1650 \text{ m}$ at $t = 5$ days), as with no solar radiation.

Typical marine low stratus clouds and fog would have LWC values in the $0.05\text{--}0.6 \text{ gm}^{-3}$ range, according to Lowmann et al. [20], so g/kg values $0.04\text{--}0.5$. Our modeled clouds are not precipitating but do have gravitational settling (0.005 ms^{-1}). With no solar radiation, our model QL values ($\sim 1 \text{ g/kg}$) are rather high, while our first estimates for QL with solar impacts ($\sim 0.03 \text{ g/kg}$) are a little low. However, Isaac et al. [21], in their Figure 12, report groups of fog cases over the Grand Banks, at a height of 69 m , with LWC in ranges of $0.005\text{--}0.01$ and $0.01\text{--}0.05 \text{ gm}^{-3}$, and so our $QL = 0.03 \text{ g/kg}$, $LWC = 0.025 \text{ gm}^{-3}$, may be

realistic while 1.0 g/kg is too high and we may need to assume larger droplet sizes and possibly allow rain to develop.

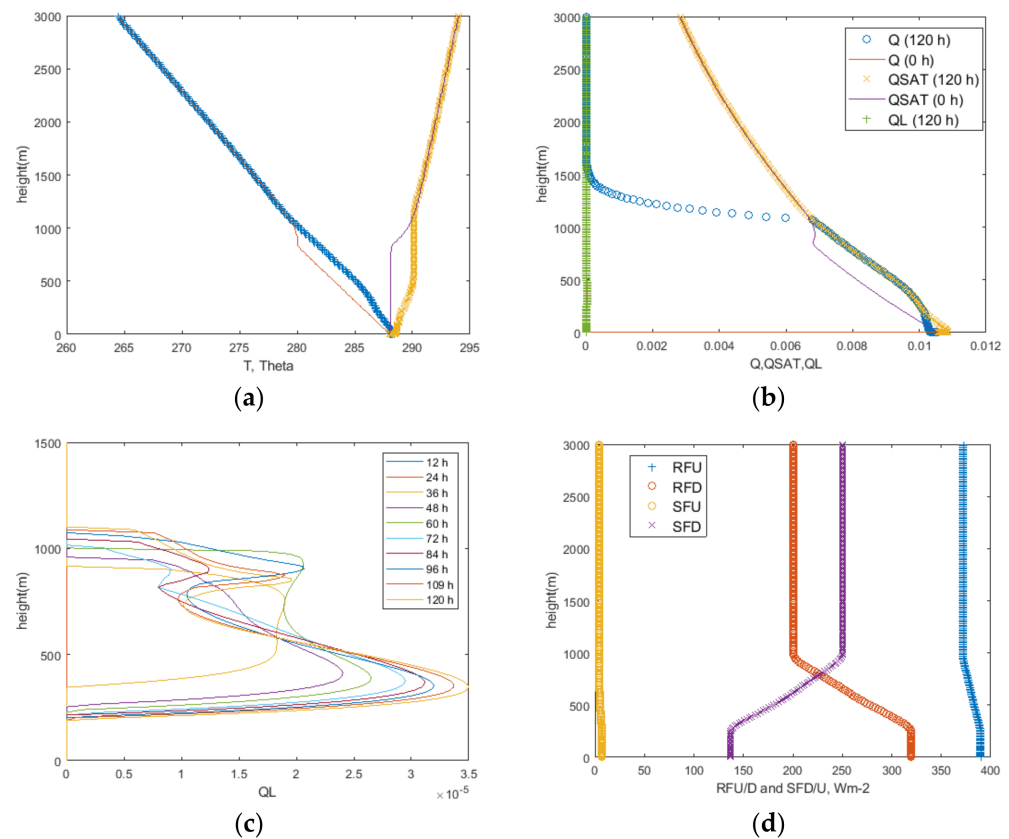


Figure 11. Selected results with long- and short-wave radiation after 120 h. (a) Temperature and potential temperature (K), (b) mixing ratios (kg/kg) (c) Liquid water mixing ratio(kg/kg), (d) radiative fluxes (Wm^{-2}).

4. Conclusions

It seems easy to understand why marine clouds occur, but a simple model suggests that the oceans should almost always be cloud covered. Solar radiation, heating, and rainout will allow clear skies at times, along with subsidence. The simple model developed and applied here may give some indication of the processes involved in warm stratus clouds and potentially can be extended to a broader range of conditions.

The essential features are that with moderate or strong winds over an extended water surface, boundary-layer mixing can lead to saturated air at some height above the surface and that this simple model predicts that, even with completely dry air to start with, clouds will form. Oliver et al. [11] suggest that “long-wavelength cooling of the water-vapor-laden air will then lead to condensation somewhere within the layer”. While that may play a role, our argument would be that the development of a layer with well-mixed water vapor and potential temperature is sufficient to generate cloud and that long-wave radiation from cloud droplets is more important than that from water vapor. Long-wave, infra-red radiation from cloud droplets then leads to cloud top cooling and an essentially stable cloud layer. If solar radiation is added, this will modify the cloud profile, but stable cloud layers may still occur.

Further work is needed to better represent solar radiation impacts and to refine other aspects of the model, including appropriate initial humidity conditions to allow more rapid cloud development. The initial aerosol distribution will have a strong impact on the droplet numbers and size distribution. We may need more information than simply QL. A simple model of raindrop formation via collision and coalescence is also needed in order to

develop a full life cycle for water evaporating from and eventually returning to the surface as rain.

Funding: This research was partially supported by a Discovery Grant from the Natural Sciences and Engineering Research Council of Canada, grant number RGPIN-2018-05947.

Institutional Review Board Statement: Not applicable.

Informed Consent Statement: Not applicable.

Data Availability Statement: Data available on request due to restrictions eg privacy or ethical. The data presented in this study are available on request from the corresponding author.

Acknowledgments: The model described and used here is based on a PBL model code developed jointly with Wensong Weng.

Conflicts of Interest: The author declares no conflict of interest.

References

1. Fog and Turbulence Interactions in the Marine Atmosphere. Available online: <https://efmlab.nd.edu/research/Fatima/> (accessed on 19 February 2024).
2. Taylor, P.A.; Chen, Z.; Cheng, L.; Afsharian, S.; Weng, W.; Isaac, G.A.; Bullock, T.W.; Chen, Y. Surface deposition of marine fog and its treatment in the Weather Research and Forecasting (WRF) model. *Atmos. Chem. Phys.* **2021**, *21*, 14687–14702. [CrossRef]
3. Cheng, L.; Chen, Z.; Taylor, P.; Chen, Y.; Isaac, G. Fog over Sable Island. CMOS Bulletin SCMO, 21 June 2021. Available online: <https://bulletin.cmos.ca/fog-over-sable-island/> (accessed on 7 May 2024).
4. MSC's Aerological Program Ends After 75 Years of Service – WSA Sable Island 1944–2019. Available online: <https://sableislandinstitute.org/mscs-aerological-program-ends/> (accessed on 7 May 2024).
5. Katata, G.; Kajino, M.; Hiraki, T.; Aikawa, M.; Kobayashi, T.; Nagai, H. A method for simple and accurate estimation of fog deposition in a mountain forest using a meteorological model. *J. Geophys. Res.* **2011**, *116*, D20102. [CrossRef]
6. Katata, G. Fogwater deposition modeling for terrestrial ecosystems: A review of developments and measurements. *J. Geophys. Res. Atmos.* **2014**, *119*, 8137–8159. [CrossRef]
7. Garratt, J.R. *The Atmospheric Boundary Layer*; Cambridge University Press: Cambridge, UK, 1992; 316p.
8. Fisher, E.L.; Caplan, P. An experiment in numerical prediction of fog and stratus. *J. Atmos. Sci.* **1963**, *20*, 425–437. [CrossRef]
9. Ballard, S.; Golding, B.; Smith, R. Mesoscale model experimental forecasts of the Haar of northeast Scotland. *Mon. Weather Rev.* **1991**, *119*, 2107–2123. [CrossRef]
10. Cotton, W.R.; Anthes, R.A. *Storm and Cloud Dynamics*; Academic Press: Cambridge, MA, USA, 1989; 880p.
11. Oliver, D.A.; Lewellen, W.S.; Williamson, G.G. The Interaction between Turbulent and Radiative Transport in the Development of Fog and Low-Level Stratus. *J. Atmos. Sci.* **1978**, *35*, 301–316.
12. Bott, A.; Trautmann, T. PAFOG—A new efficient forecast model of radiation fog and low-level stratiform clouds. *Atmos. Res.* **2002**, *64*, 191–203. [CrossRef]
13. Wainwright, C.; Richter, D.H. Investigating the sensitivity of marine fog to physical and microphysical processes using large-eddy simulation. *Bound.-Layer Meteorol.* **2021**, *181*, 473–498. [CrossRef]
14. Koračin, D.; Lewis, J.; Thompson, W.T.; Dorman, C.E.; Businger, J.A. Transition of Stratus into Fog along the California Coast: Observations and Modeling. *J. Atmos. Sci.* **2001**, *58*, 1714–1731. [CrossRef]
15. Koračin, D.; Rogers, D.P. Numerical simulations of the response of the marine atmosphere to ocean forcing. *J. Atmos. Sci.* **1990**, *47*, 592–611. [CrossRef]
16. Rogers, D.P.; Koračin, D. Radiative transfer and turbulence in the cloud-topped marine atmospheric boundary layer. *J. Atmos. Sci.* **1992**, *49*, 1473–1486. [CrossRef]
17. Weng, W.; Taylor, P.A. On modelling the 1-D atmospheric boundary layer. *Bound.-Layer Meteorol.* **2003**, *107*, 371–400. [CrossRef]
18. Stevens, G.L. The Parameterization of Radiation for Numerical Weather Prediction and Climate Models. *Mon. Weather Rev.* **1984**, *112*, 826–867. [CrossRef]
19. Brown, R.; Roach, W.T. The physics of radiation fog. II. A numerical study. *Q. J. R. Meteorol. Soc.* **1976**, *102*, 335–354.
20. Lohmann, U.; Lüönd, F.; Mahrt, F. *An Introduction to Clouds: From the Microscale to Climate*; Cambridge University Press: Cambridge, UK, 2016; 391p.
21. Isaac, G.A.; Bullock, T.; Beale, J.; Beale, S. Characterizing and Predicting Marine Fog Offshore Newfoundland and Labrador. *Weather Forecast.* **2020**, *35*, 347–365. [CrossRef]

Disclaimer/Publisher's Note: The statements, opinions and data contained in all publications are solely those of the individual author(s) and contributor(s) and not of MDPI and/or the editor(s). MDPI and/or the editor(s) disclaim responsibility for any injury to people or property resulting from any ideas, methods, instructions or products referred to in the content.